Supporting information

Fabrication and Electrochemical Evaluation of Flexible Spinel $CdMn_2O_4$ Carbon Nanofibers for Advanced Supercapacitor Applications

Akash P. Patel[a], Deep S. Sharma[a], Sanjay N. Bariya[b], Yash G. Kapdi[b], Jaydip D. Solanki[c], Saurabh S. Soni[b], Vaibhav K. Patel[a,d]*, Sanjay H. Panjabi[a]*

[a] Department of Chemical Sciences, P D Patel Institute of Applied Sciences, Charotar University of Science and Technology, Changa - 388421, Gujarat, INDIA.

[b] Department of Chemistry, Sardar Patel University, Vallabh Vidyanagar - 388120, Gujarat, INDIA.

[c] Department of Applied and Interdisciplinary Sciences (IICISST), Sardar Patel University, Vallabh Vidyanagar 388120, Gujarat, India

[d] The Charutar Vidya Mandal (CVM) University, Anand - 388120, Gujarat, INDIA.

*Corresponding Author: sanjaypanjabi_27@yahoo.co.in

Corresponding Author 2: vaibhav272@yahoo.co.in

Electrochemical Performance Measurements

The electrochemical studies of the spinel $CdMn_2O_4$ CNFs were performed using an electrochemical workstation (CHI660E) in a 6M KOH and 1M H_2SO_4 aqueous electrolyte solution. The experiment involved utilizing a conventional three-electrode setup, with the $CdMn_2O_4$ CNFs serving as the working electrode, Ag/AgCl with 3.0 M KCl as the reference electrode, and platinum wire as the counter electrode. Cyclic Voltammetry (CV) was performed at different scan rates, galvanostatic charge-discharge (GCD) was performed at various current densities, and EIS was conducted in the frequency range of 100 kHz to 0.1 Hz with an AC amplitude. Two methods are employed to determine the specific capacitance in a three-electrode configuration: CV and GCD.

For CV, the specific capacitance (Cs) is computed using equation (S1):[1]

$$C_s = \frac{1}{mv(E_2 - E_1)} \int_{E_1}^{E_2} i(E)dE \#(S1)$$

Where the difference between E_2 and E_1 represents the potential window. The variable m represents the mass of the active synthesized material, v denotes the scan rate, and i(E) represents the current at each potential.

For GCD, the specific capacitance (Cs) is determined using equation (S2):

$$C_s = \frac{I \times \Delta t}{m \times \Delta V} \#(S2)$$

Where Cs represents the specific capacitance in ($F.g^{-1}$), I stands for the current in (A), Δt denotes the time interval in seconds for discharge, ΔV and m represents the voltage window (V) and mass of active material in (g).

Two-electrode systems evaluated the properties of a symmetrical solid-state supercapacitor. The specific capacitances of a single electrode were calculated based on the GCD outcomes using the following equation (S3):[2]

$$C_s = \frac{4 \times I \times \Delta t}{m \times \Delta V} \#(S3)$$

The energy density (E, Wh kg^{-1}) and power density (P, W kg^{-1}) of the fabricated SSC device were calculated by the following formulas:

$$E = \frac{1}{2} C_s V^2 \times \frac{1}{3600 \times m} \#(S4)$$

$$P = \frac{E \times 3600}{t_{discharge}} \#(S5)$$

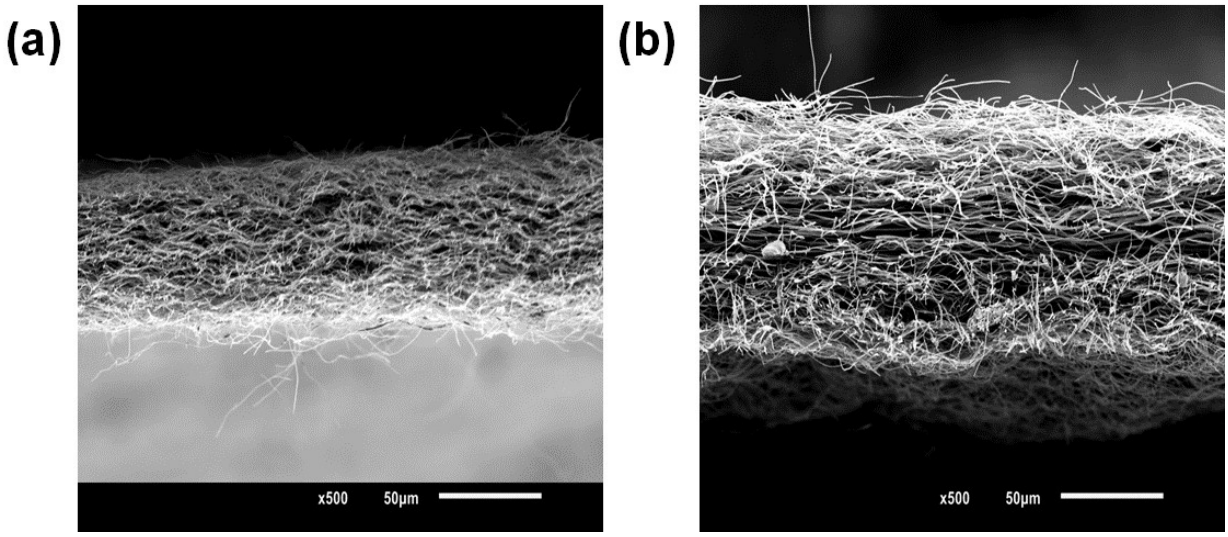

Figure S1. Cross-sectional SEM image of (a) CMO-1 and (b) CMO-2

The thickness of CMO-1 is approximately 67 µm, whereas CMO-2 has a thickness of around 88 µm.

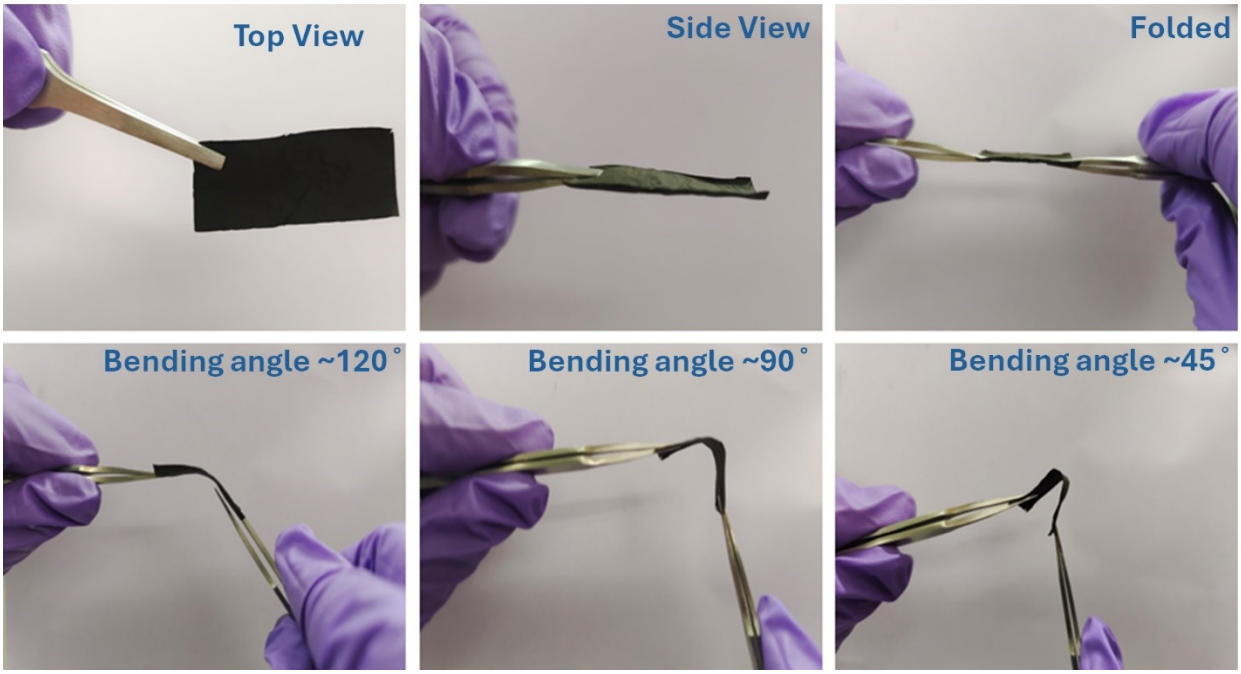

Figure S2. Photographic Images of spinel $CdMn_2O_4$ carbon nanofibers(CNFs)

Figure S2 shows images of the spinel $CdMn_2O_4$ CNFs at different angles, demonstrating the thickness and flexibility of the material. This visual representation provides valuable insights into the physical characteristics of the flexible material, showcasing its structural properties from various perspectives.

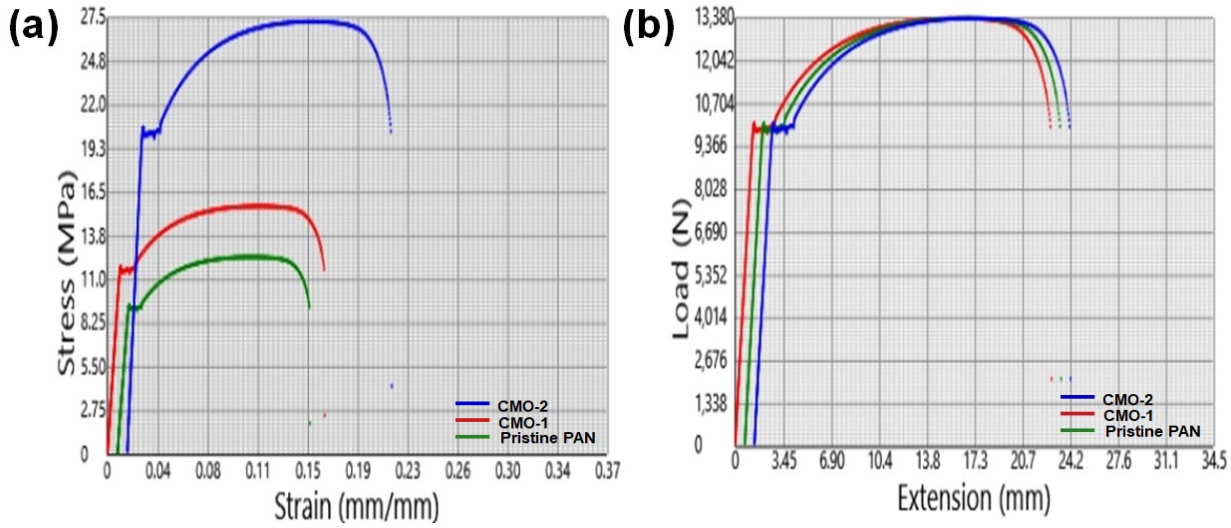

Figure S3. Stress-strain and load-extension curves for Pristine PAN, CMO-1,and CMO-2 CNFs.

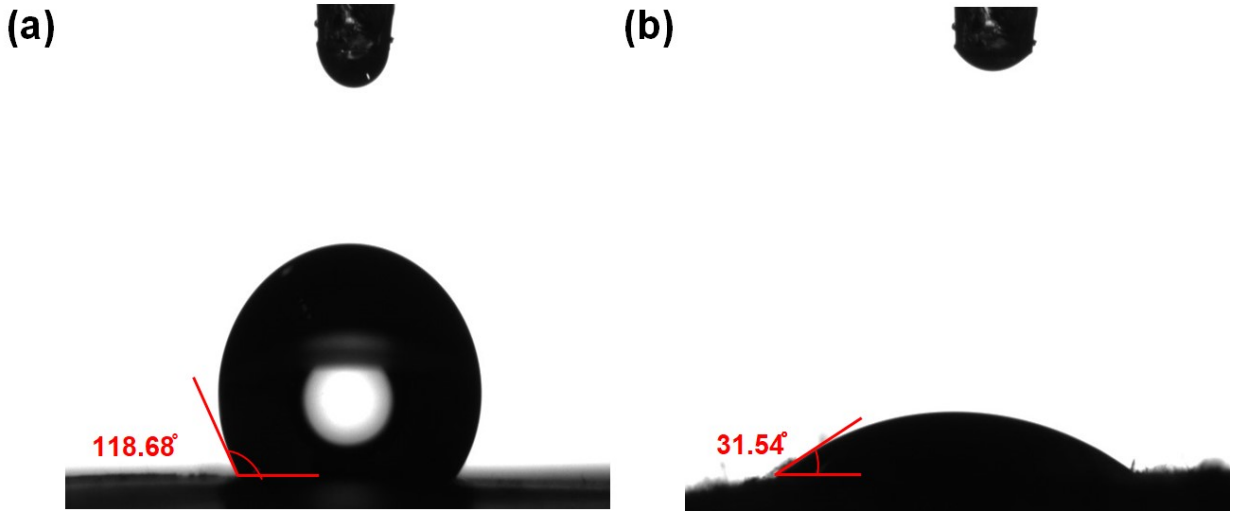

Figure S4. Contact angle of a water droplet on the surface of (a) Pristine PAN carbon nanofibers and (b) $CdMn_2O_4$ carbon nanofiber

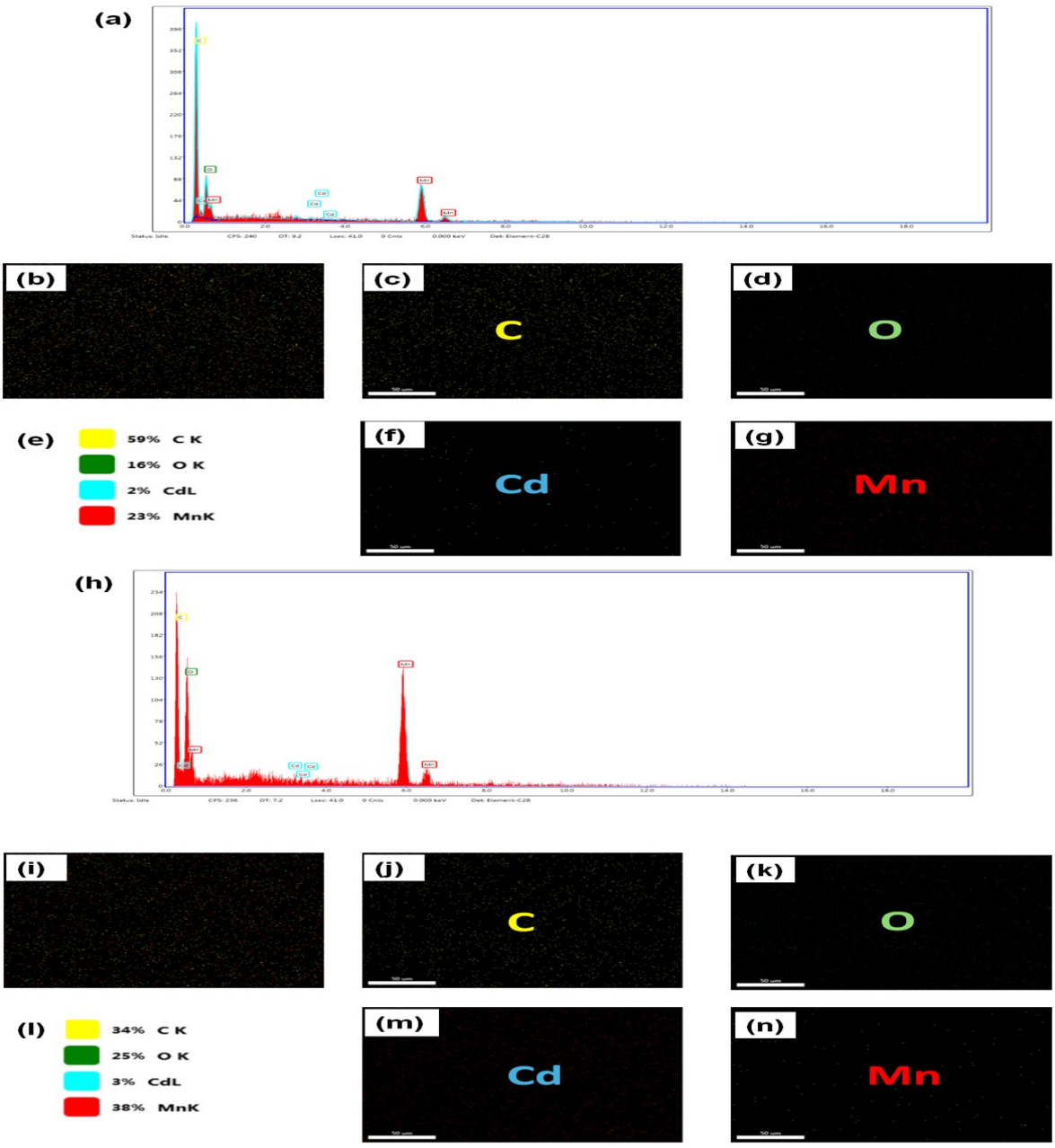

Figure S5. (a-g) presents the EDAX analysis for CMO-1, including (e) the EDAX spectrum showing the percentage of chemical elements present. (c-g) display the elemental mapping images for the individual distribution of C, O, Cd, and Mn, respectively. (h-n) presents the EDAX analysis for CMO-2, including (l) the EDAX spectrum showing the percentage of chemical elements present.

(j-n) display the elemental mapping images for the individual distribution of C, O, Cd, and Mn, respectively.

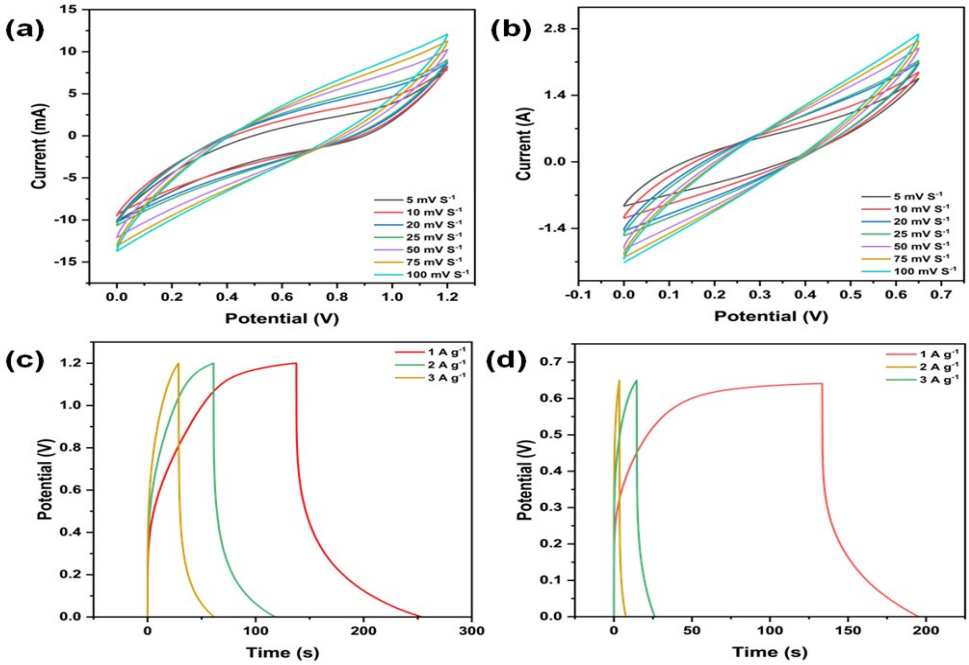

Figure S6.CV curves at varying scan rates (a, b) and GCD curves at different current densities (c, d) of Pure MnO_2

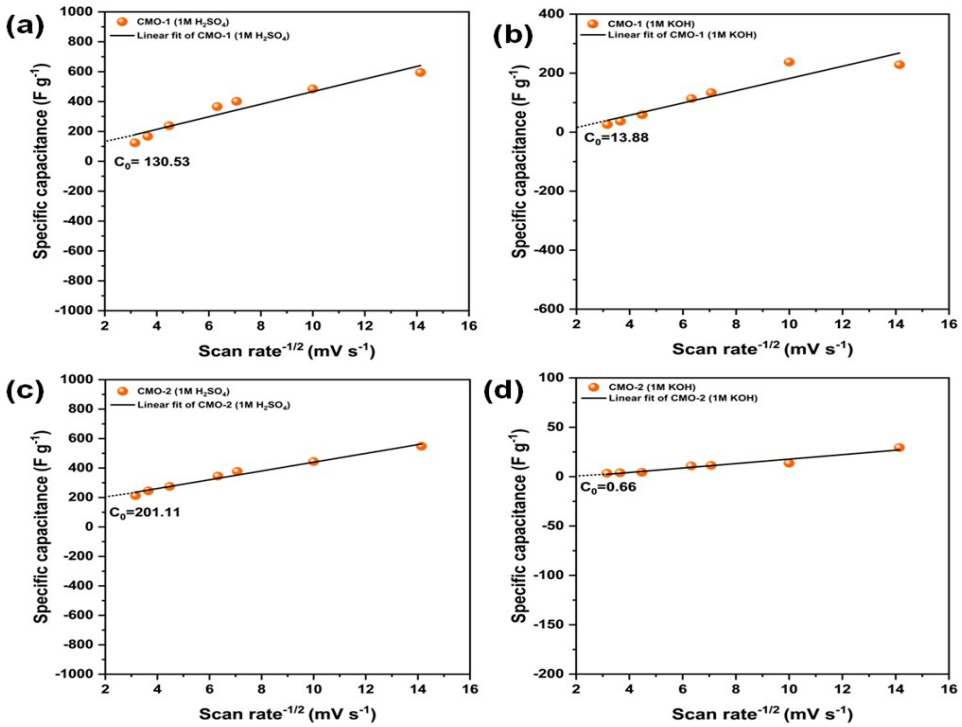

Figure S7. Specific capacitance vs. scan rate$^{-1/2}$ for (a-b) CMO-1 and (c-d) CMO-2 in 1M H_2SO_4 and 1M KOH, with linear fits showing C_o values

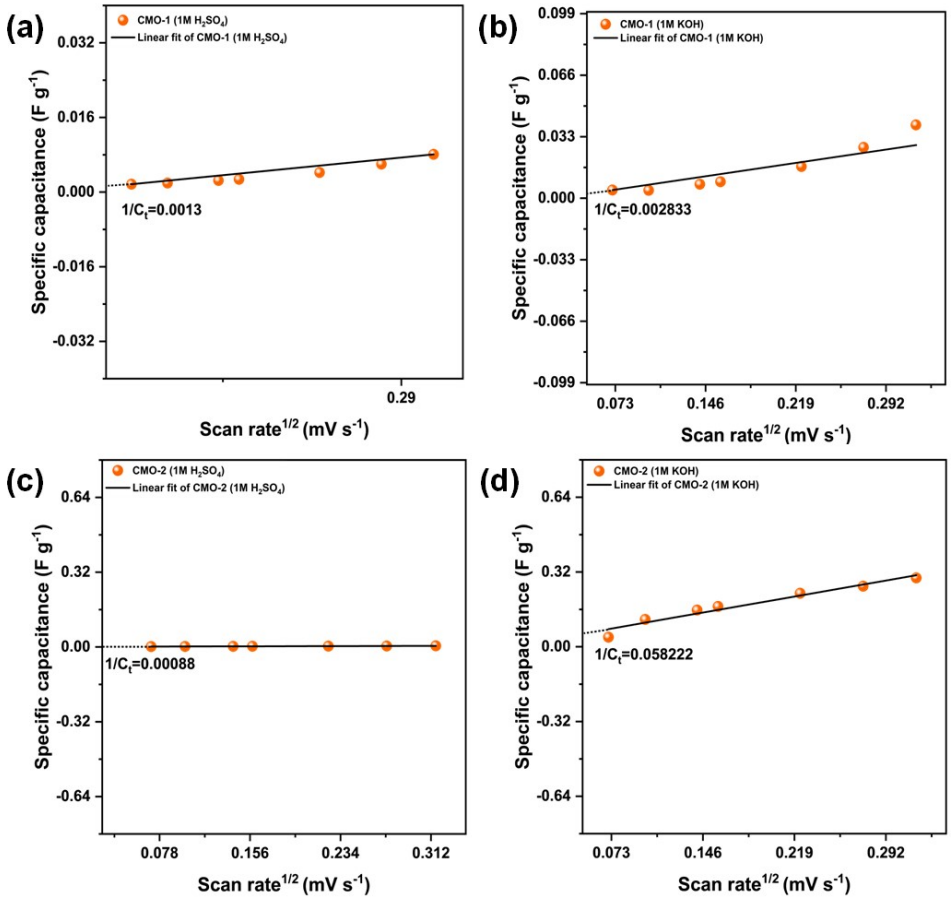

Figure S8. Specific capacitance vs. scan rate$^{1/2}$ for (a-b) CMO-1 and (c-d) CMO-2 in 1M H_2SO_4 and 1M KOH, with linear fits showing C_t values.

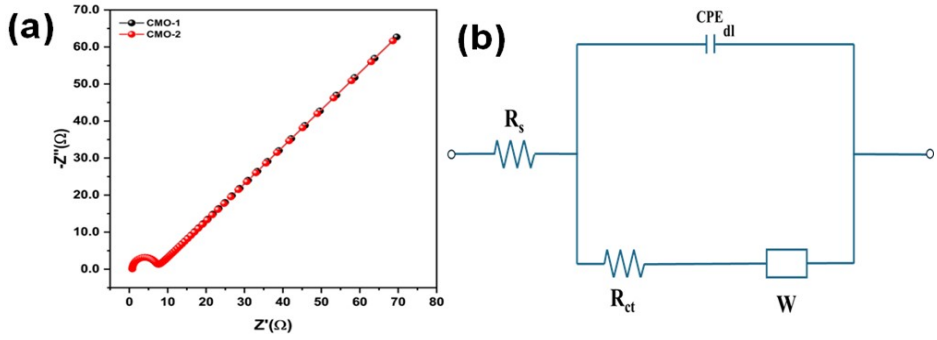

Figure S9. Nyquist plots of CMO-1 and CMO-2 in (a) 1M H_2SO_4 and (b) 1M KOH using a three-electrode setup, showing impedance behavior of the materials. (c) Fitted equivalent circuit

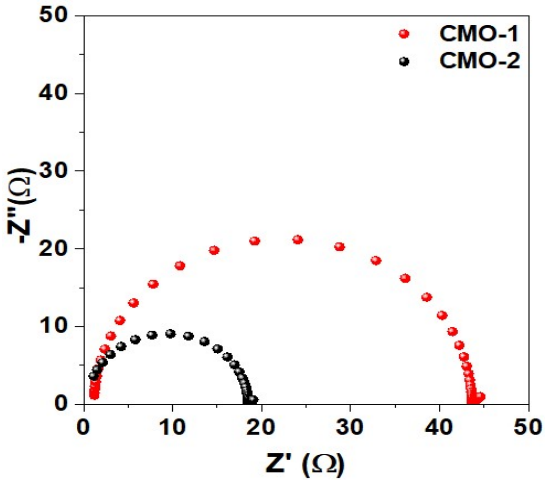

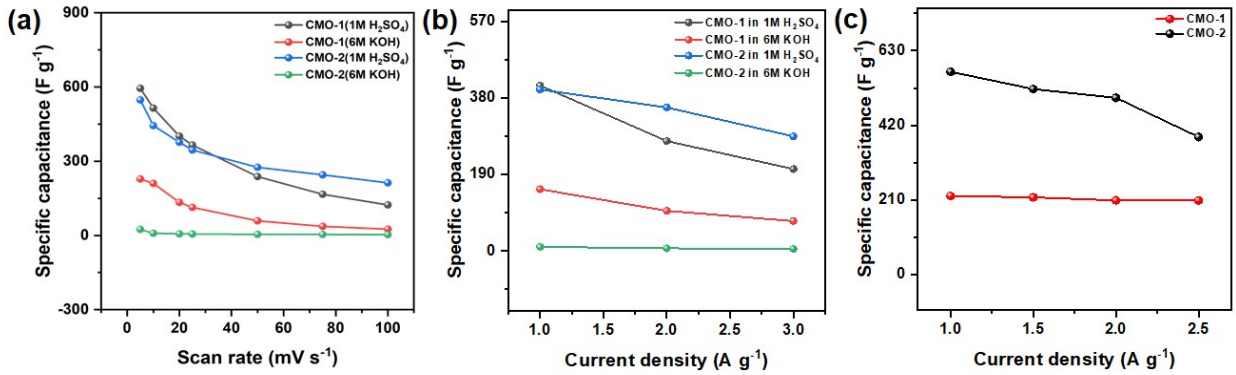

Figure S10. Nyquist plots of CMO-1 and CMO-2 CNFs

Figure S11. (a) Variation of calculated specific capacitance with scan rate, (b) Variation of calculated specific capacitance with current density for CMO-1 and CMO-2 in two different electrolytes and (c) Variation of calculated specific capacitance with current density for CMO-1 and CMO-2 of solid state symmetric supercapacitor

Figure S11(a) shows specific capacitance variation with scan rate for CMO-1 and CMO-2 in different electrolytes, providing insight into supercapacitor performance. Figure S11(b) depicts specific capacitance variation with current density for CMO-1 and CMO-2 in two electrolytes, offering information on behaviour at different charging rates. Figure S11(c) illustrates specific capacitance variation with current density for CMO-1 and CMO-2 in a solid-state symmetric supercapacitor, providing data on performance under different operating conditions.

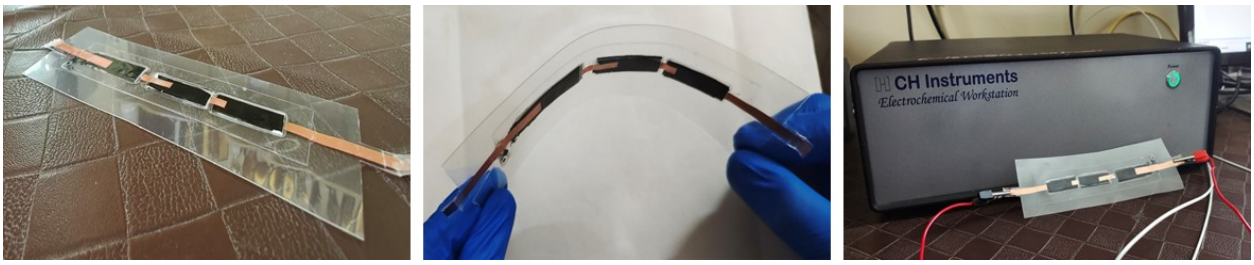

Figure S12. Photographic images of real-time flexible devices

Figure S12 presents photographic images of real-time flexible devices. The images likely depict the actual flexible supercapacitor devices based on the spinel CdMn2O4 carbon nanofibers. These images are crucial for demonstrating the supercapacitor devices in real-world application and flexibility. The devices flexibility is an essential characteristic that can contribute to their potential use in various flexible and portable electronic applications.

Table S1. ICP-OES elemental analysis of CMO-1 and CMO-2 showing the concentration of key elements (in ppm).

Element	CMO-1	CMO-2
Al	0.198	0.223
B	0.208	0.278
Cd	685.233	712.236
Co	0.022	0.020
Mn	528.413	1442.127
Ni	0.024	0.022
Se	0.197	0.370
V	0.005	0.011
Zn	0.080	0.097

Table S2. Comparison of three electrode data of reported MnO_2-based electrode material and Spinel $CdMn_2O_4$ carbon nanofiber.

Electrode Material	**Specific Capacitance**	**Scan Rate/Current Density**	**Voltage window**	**Electrolyte**	**Reference**
α-MnO_2 nanorod	166.22 F g^{-1}	10 mV S^{-1}	0 V-1.0V	0.1 M Na_2SO_4	[3]

Carbon nanofiber/MnO_2	151.1 F g^{-1}	1 A g^{-1}	-0.2 V – 0.8V	1.0 M Na_2SO_4	[4]
MnO_2/carbon nanotubes–embedded carbon nanofibers	374 F g^{-1}	2 mV S^{-1}	0 V-0.9V	0.1 M Na_2SO_4	[5]
Mn_2O_3@MnO_2 composite nanofibers	190 F g^{-1}	1 A g^{-1}	0 V-1.0V	1.0 M Na_2SO_4	[6]
MnO_x Nanofiber	214.7 F g^{-1}	10 mV S^{-1}	-0.2 V – 0.8V	0.5 M Na_2SO_4	[7]
Spinel $CdMn_2O_4$ nanofiber	210 F g^{-1}	1 A g^{-1}	0 V-1.0V	1.0 M Na_2SO_4	[8]
Spinel $CdMn_2O_4$ carbon nanofiber	For CMO-1-594.7 F g^{-1} For CMO-2-547.64 F g^{-1}	5 mV S^{-1}	0 V -1.2 V	1.0 M H_2SO_4	This Work

Table S3. Impedance parameters for CMO-1 and CMO-2 derived from electrochemical impedance spectroscopy (EIS) analysis in both three-electrode and symmetric solid-state supercapacitor configurations

Configuration	**sample**	**Rs**	**Rct**	**C**	**W**
3 Electrode	**CMO-1**	0.787	6.13	2.826E-6	0.01423
	CMO-2	0.8001	6.187	2.902E-6	0.01448
2 Electrode	**CMO-1**	1.981	224.9	1.209E-5	0.008733
	CMO-2	1.486	360.5	1.280E-5	0.00542

References

1 D. S. Sharma, A. P. Patel, S. N. Bariya, Y. G. Kapdi, S. S. Soni, N. N. Patel, S. H. Panjabi and V. K. Patel, *ACS Appl. Electron. Mater.*, 2024, **6**, 3617–3629.

2 B. Y. Pathak, S. Zinzuvadiya, S. Pachauri, S. N. Bariya, S. S. Soni and U. S. Joshi, *Electrochim. Acta*, 2024, **492**, 144309.

3 Y. Li, H. Xie, J. Wang and L. Chen, *Mater. Lett.*, 2011, **65**, 403–405.

4 P. Ning, X. Duan, X. Ju, X. Lin, X. Tong, X. Pan, T. Wang and Q. Li, *Electrochim. Acta*, 2016, **210**, 754–761.

5 J. G. Wang, Y. Yang, Z. H. Huang and F. Kang, *Electrochim. Acta*, 2012, **75**, 213–219.

6 W. Lu, Y. Li, M. Yang, X. Jiang, Y. Zhang and Y. Xing, *ACS Appl. Energy Mater.*, 2020, **3**, 8190–8197.

7 E. Lee, T. Lee and B. S. Kim, *J. Power Sources*, 2014, **255**, 335–340.

8 J. Bhagwan, A. Sahoo, K. L. Yadav and Y. Sharma, *J. Alloys Compd.*, 2017, **703**, 86–95.